Stability Limits and Improved Robustness of Grid-Forming Converters With External Inertia-Emulation Loop

Downloaded from: https://research.chalmers.se, 2025-09-25 08:18 UTC

Citation for the original published paper (version of record):

Imgart, P., Bongiorno, M., Svensson, J. et al (2023). Stability Limits and Improved Robustness of Grid-Forming Converters With External
Inertia-Emulation Loop. 2023 25th European Conference on Power Electronics and Applications, EPE 2023 ECCE Europe. http://dx.doi.org/10.23919/EPE23ECCEEurope58414.2023.10264526

N.B. When citing this work, cite the original published paper.

research.chalmers.se offers the possibility of retrieving research publications produced at Chalmers University of Technology. It covers all kind of research output: articles, dissertations, conference papers, reports etc. since 2004. research.chalmers.se is administrated and maintained by Chalmers Library

(article starts on next page)

Stability Limits and Improved Robustness of Grid-Forming Converters With External Inertia-Emulation Loop

Paul Imgart[1], Massimo Bongiorno[1], Jan R. Svensson[2], Mebtu Beza[1]
paul.imgart@chalmers.se

(1): Chalmers University of Technology
Dept. of Electrical Engineering
Göteborg, Sweden

(2): Hitachi Energy
Hitachi Energy Research
Västerås, Sweden

***Index Terms*—Grid-forming converter, inertia support, synchronization stability, low-inertia grid, robustness.**

***Abstract*—An external inertia emulation loop (IEL) prevents instability in grid-forming converters during frequency disturbances. This paper investigates IEL stability limits and compares three alternatives to improve IEL performance under power limitation. Simulations confirm the IEL's robustness and the effectiveness of the proposed solution in avoiding undesired active-power injection at the disturbance end.**

I. Introduction

The world-wide transformation towards sustainable power grids is leading to an increased share of grid-connected power electronics, which challenges the grid stability. Grid-forming (GFM) converter control is the preferred solution discussed for these challenges, since the converter behaves as a slowly changing voltage source. This behaviour allows the converter to enhance grid stability for example by providing inertial response or short-circuit current [1], [2]. However, this behavior can also give rise to control instability during grid disturbances and in particular when the converter current is to be limited [3]. To deal with these instabilities and preserve the GFM behaviour in all operating conditions, a cascaded power controller (CPC) has been proposed in [4] and [5]. This controller consists of a fast active-power loop (APL) for reference tracking and synchronization, and an inertia-emulation loop (IEL), which generates the desired inertial response as part of the APL's reference. As shown in [4], [5], the CPC significantly increases the robustness of the converter system against grid frequency disturbances.

While the effectiveness of the CPC in providing grid support and at the same time maintaining synchronous operation of the converter even in case of extreme grid disturbances has been established, the stability limits of this control strategy have not been investigated yet. The tests conducted in [5] have shown that the CPC is robust even for a high rate of change of frequency (ROCOF), but it is important to understand at which ROCOF the CPC loses the ability to track the grid voltage angle for a given inertia constant. This can be relevant in particular for operation in weak grids, where the local ROCOF can deviate notably from the system ROCOF experienced at the center of inertia, putting high stress on the GFM converter [6]. Furthermore, it is important to consider that GFM converters in future grids can be required to operate with inertia constants much higher than typical for synchronous machines, up to several tens of seconds, which can reduce the stability margin of the CPC. An example for an application with a high inertia constant could be a large offshore wind farm combined with an GFM controlled energy-storage equipped static compensator (ES-STATCOM) to provide inertial support and other ancillary services [7].

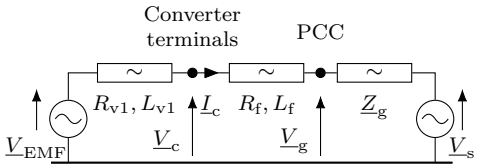

Fig. 1: Investigated system setup.

The aim of this paper is to understand possible stability limits for the IEL in terms of maximum ROCOF and emulated inertia, and to provide suitable modifications to the original IEL controller. After a theoretical investigation of the IEL robustness, three alternatives to improve the IEL are presented and compared through time-domain simulations.

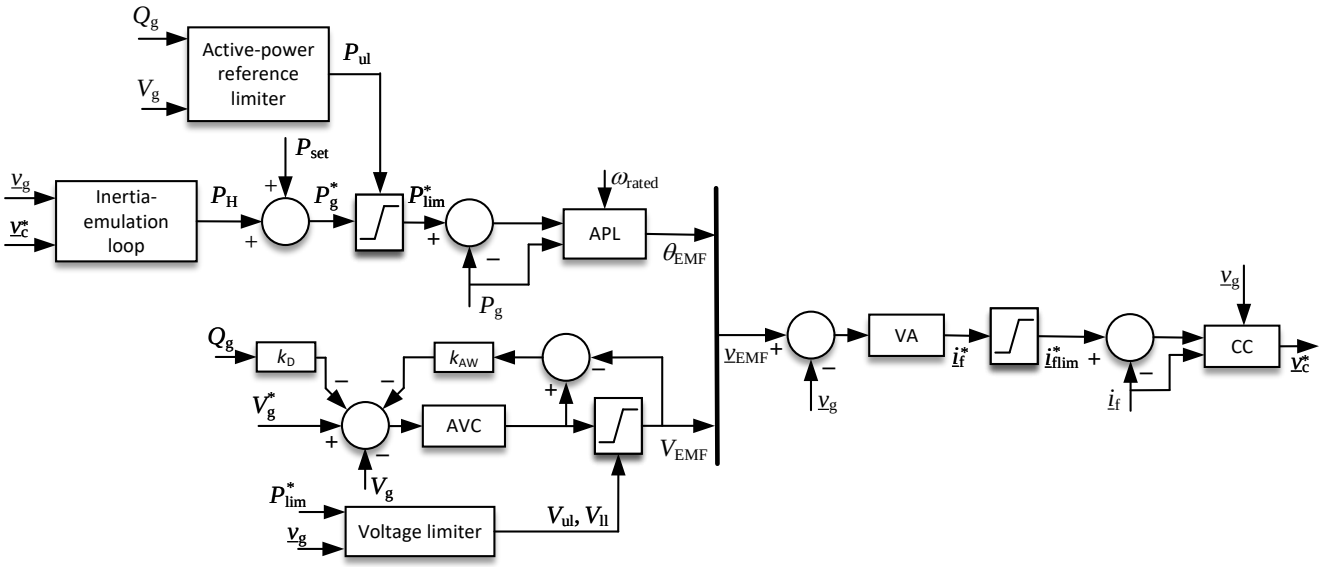

Fig. 2: Block diagram of the investigated GFM converter control with CPC [5].

II. IEL Stability Limits

The theoretical stability limits of the IEL are analyzed using the system depicted in Fig. 1, and the converter control presented in [5] and shown in Fig. 2. The controller is a virtual admittance-based GFM converter controller, with a CPC consisting of a fast APL and an IEL, an AC voltage controller, a virtual admittance (VA) and a current controller. In this controller, a voltage-based current limitation is employed, based on the limitation of the active power reference and virtual back EMF magnitude to prevent current-limiter induced instability as described in [5]. The IEL enables effective limitation of the APL's power reference by providing the desired inertial response as part of the reference; its structure is presented in Fig. 3. The proportional gain $K_{\mathrm{p,IEL}}$ and the integral gain $K_{\mathrm{i,IEL}}$ of the IEL are tuned following the procedure from [4] and depend on the desired inertia constant and damping:

$$K_{\mathrm{p,IEL}} = \zeta\sqrt{\frac{2\omega_{\mathrm{b}}L_{\mathrm{f}}}{H}} \quad \text{and} \quad K_{\mathrm{i,IEL}} = \frac{\omega_{\mathrm{b}}}{2H}, \tag{1}$$

where ζ is the damping ratio of the inertial response, ω_{b} is the nominal angular frequency of the grid voltage, L_{f} is the converter filter inductance in pu and H is the inertia constant emulated by the IEL.

In a weak grid, the IEL indirectly influences the grid voltage by changing the active power reference. This interaction will alter the ROCOF experienced at the grid connection point by the converter. To reduce unnecessary complexity and investigate the worst case, an infinitely strong grid is assumed here.

As can be seen from the IEL block diagram in Fig. 3, the inertial power P_{H} is determined by

$$P_{\mathrm{H}} = -\frac{v_{\mathrm{gq,IEL}}V_{\mathrm{c}}^*}{L_{\mathrm{f}}}, \tag{2}$$

where V_{c}^* is the magnitude of the converter voltage reference in pu and $v_{\mathrm{gq,IEL}}$ is the q-component of the grid voltage in pu in the IEL reference frame. The latter is given as

$$v_{\mathrm{gq,IEL}} = V_{\mathrm{g}}\sin(\delta_{\mathrm{IEL}}), \tag{3}$$

where V_{g} is the grid voltage magnitude and $\delta_{\mathrm{IEL}} = \theta_{\mathrm{g}} - \theta_{\mathrm{IEL}}$ is the angle difference between the grid voltage vector phase angle θ_{g} and the internal IEL angle θ_{IEL}. Consequently, the IEL tracks the grid angle with a bandwidth determined by L_{f} and the parameters of the PI-controller. In steady-state, δ_{IEL} (and consequently P_{H}) is zero; in case of phase-angle jumps or grid frequency excursions however, the result is a non-zero angle difference δ_{IEL}, causing an inertial response. This inertial response is proportional to the size of the phase-angle jump or the ROCOF, respectively, and thereby

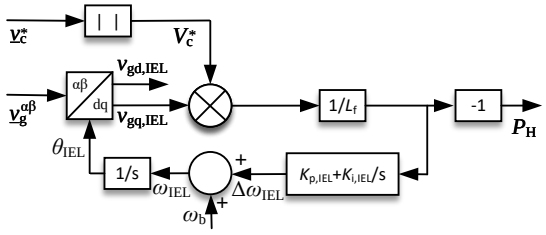

Fig. 3: Block diagram of the IEL [5].

mimics the mechanical inertia of a synchronous machine. To achieve this, the presence of an angle difference as a reaction to a ROCOF is intentional. The IEL is a second-order controller, and a constant ROCOF results in a constant angle difference.

Depending on the ROCOF, selected inertia, and active power set-point P_{set}, the sum of P_{set} and inertial response P_{H} can exceed the active power capacity of the converter. In this case the active power reference needs to be limited. This is also the case in presence of voltage disturbances, such as voltage dips, when reactive power might need to be prioritized. Under active power reference limitation, δ_{IEL} exceeds the value that is required to provide the actual available inertial response given by $P_{\mathrm{lim}} - P_{\mathrm{set}}$. This results in an active power injection that continues even after the frequency disturbance subsides. A large angle difference δ_{IEL} can also lead to IEL instability. Both problems are investigated in detail in continuation.

A. IEL Instability

To determine at which ROCOF an IEL with a given tuning loses the ability to track the grid voltage angle, an analysis of the controller in Fig. 3 that takes the non-linearity into account is neccessary. The internal IEL frequency ω_{IEL} and the angle separation δ_{IEL} are determined by

$$\omega_{\mathrm{IEL}} = \frac{1}{L_{\mathrm{f}}}\Bigg(K_{\mathrm{p,IEL}} V_{\mathrm{c}} v_{\mathrm{gq,IEL}} + K_{\mathrm{i,IEL}} \int V_{\mathrm{c}} v_{\mathrm{gq,IEL}}\, \mathrm{d}t\Bigg) + \omega_{\mathrm{b}} \tag{4}$$

$$\delta_{\mathrm{IEL}} = \int (\omega_{\mathrm{g}} - \omega_{\mathrm{IEL}})\, \mathrm{d}t + \theta_{\mathrm{g0}}, \tag{5}$$

where ω_{g} is the grid frequency. With the aim to identify the critical ROCOF that causes IEL instability, the voltage magnitudes V_{c} and V_{g} are assumed to be constant. Under these conditions, differentiating (4) by time results in

$$\dot{\omega}_{\mathrm{IEL}} = \frac{1}{L_{\mathrm{f}}} \left(K_{\mathrm{p,IEL}} V_{\mathrm{c}} \dot{v}_{\mathrm{g,q}} + K_{\mathrm{i,IEL}} V_{\mathrm{c}} v_{\mathrm{gq,IEL}}\right). \tag{6}$$

If the ROCOF is constant, δ_{IEL} will approach a constant value. For this analysis, the dynamics of the inertial response are disregarded and this final value is considered, which results in $\dot{v}_{\mathrm{g,q}} = 0$. Substituting this in (6) yields

$$\dot{\omega}_{\mathrm{IEL}} = \frac{V_{\mathrm{c}} V_{\mathrm{g}}}{L_{\mathrm{f}}} K_{\mathrm{i,IEL}} \sin \delta_{\mathrm{IEL}}. \tag{7}$$

A constant angle difference requires ω_{IEL} to be equal to ω_{g}. In the constant-ROCOF case that is considered here, this results also in $\dot{\omega}_{\mathrm{IEL}} = \dot{\omega}_{\mathrm{g}}$. However, as can be seen from (7), the maximum ROCOF that the IEL can follow is reached for a δ_{IEL} of $\pm 90°$, when $\sin \delta_{\mathrm{IEL}} = 1$. This is the critical ROCOF and a larger ROCOF will result in the inability of the IEL to track the grid voltage angle, i.e. instability. From (7), the critical ROCOF is given as

$$\dot{\omega}_{\mathrm{g,crit}} = \pm \frac{V_{\mathrm{c}} V_{\mathrm{g}}}{L_{\mathrm{f}}} K_{\mathrm{i,IEL}} = \pm \frac{V_{\mathrm{c}} V_{\mathrm{g}} \omega_{\mathrm{b}}}{2 H L_{\mathrm{f}}}, \tag{8}$$

where in the second expression the integral gain has been substituted according to (1).

To illustrate this, the IEL differential equation is numerically solved with the parameters in Table I to estimate the angle separation between the grid voltage and the internal IEL angle. For this isolated simulation of the IEL, the magnitude of the grid and converter voltage are assumed to 1 pu and the inertial power reference P_{H} is limited between 0 and 1 pu. The results for a stable (ROCOF = −3 Hz/s) and an unstable (ROCOF = −3.75 Hz/s) case are shown in Fig. 4. In the stable case, the absolute value of the angle separation remains below 90° during the complete disturbance, whereas in the unstable case, the stability limit is exceeded approximately 0.75 s after the disturbance begins. As can be seen from the figure, the IEL does not lose stability at the instant the ROCOF starts, but after the disturbance has persisted for some time, during which the angle separation to grow until it surpasses the stability limit. It is important to stress that the frequency has already decreased to approximately 47 Hz at this point.

The non-negligible duration before instability occurs motivates further study of the relation between the inertia constant, the ROCOF, and the ROCOF duration causing IEL instability. For this purpose, a parameter study has been conducted based on the same numerical model. The IEL's response is simulated for a selection of inertia constants and over a wide range of ROCOFs.

The results shown in Fig. 5 are used to investigate the stability margin as a function of inertia constant and ROCOF. In the top plot, the duration of constant ROCOF it takes δ_{IEL} to surpass the stability limit of 90° is depicted, denoted as time to instability. At the bottom, instead the grid frequency at the instant when the stability limit is crossed is shown. From these results it can be

TABLE I: IEL parameters.

Parameter	Value
H	50 s
ζ	0.707
L_{f}	0.15 pu

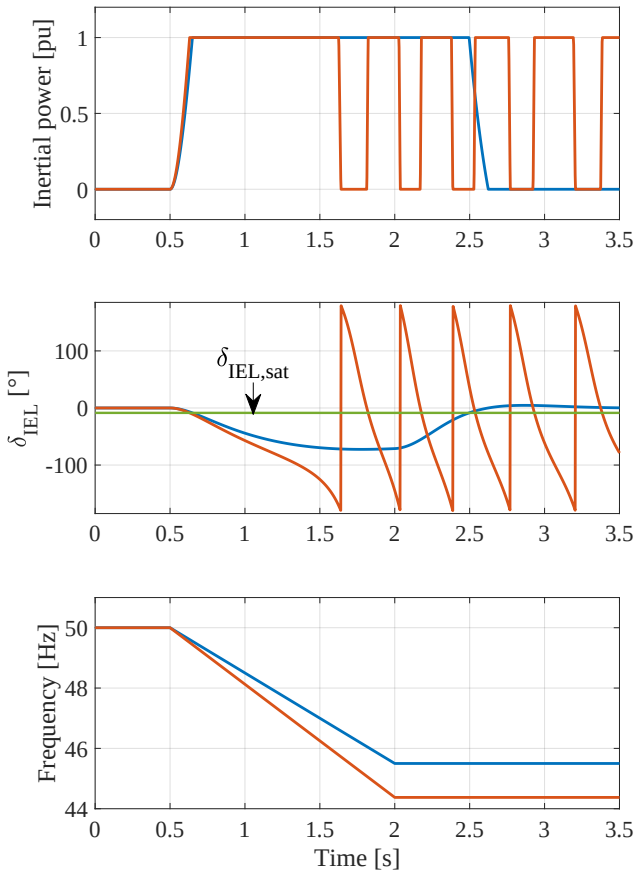

Fig. 4: Top: Limited inertial power reference for a stable (blue) and an unstable case (red). Middle: Angle separation between grid voltage angle and internal IEL angle. Bottom: Grid frequency.

concluded that the IEL is stable for all realistic ROCOF values. In conventional power plants with synchronous generators, the inertia constant is typically in the range of 2 s to 10 s [8], and in this range, IEL instability does not occur for a ROCOF and grid frequency close to the operating limits defined in current grid codes [9]. Even with the expectation that the decrease in inertia caused by an increasing share of converter-interfaced generation results in larger frequency deviations and ROCOFs in future power systems [10], risk for instability might only occur if exceptionally high inertia provision is required from the converter.

This could be the case in situations where a single GFM converter provides inertial response for a number of other units, such as an ES-STATCOM for a wind farm. In this situation, the required inertia constant – a relative value depending on the unit's rated power – can be notably higher than in today's conventional power plants. As indicated by [2], it can be expected that in future converter-dominated power grids only a minority of

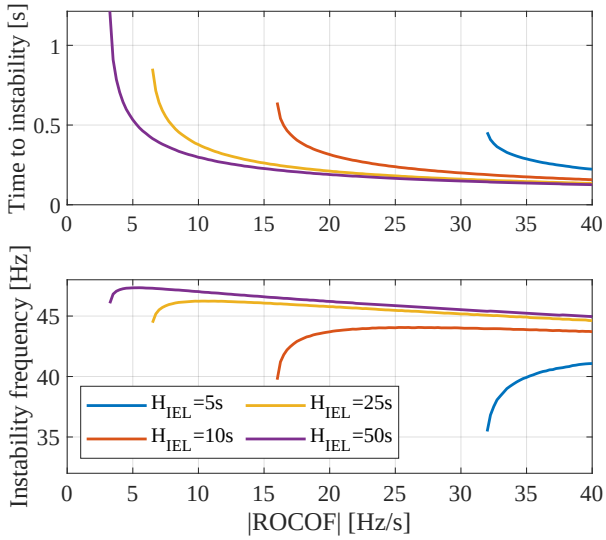

Fig. 5: Top: Estimated critical ROCOF and time to occurence of IEL instability, depending on the inertia constant. Bottom: Estimated critical ROCOF and frequency at occurence of IEL instability.

converters will have GFM capabilities, which increases the probability that unusually high inertia constants are required.

Nevertheless, Fig. 5 shows that even for an emulated inertia of 50 s, a high constant ROCOF of ±5 Hz/s can be sustained for 0.5 s before the IEL loses stability. Although it is of vital importance to guarantee stable converter operation in all feasible operating conditions, based on these considerations the main motivation for the modifications suggested in this paper lies not in the risk of IEL instability, but in the consequences of operation under power reference saturation described below.

B. IEL under power limitation

As can be seen from the stable case presented in Fig. 4, the inertial power continues to be injected for approximately 500 ms even after the ROCOF subsides. The reason for this is shown in the second plot in the same figure, where the estimated δ_{IEL} is shown. Due to the large ROCOF, the angle difference is much larger than what is needed to achieve the maximum possible inertial power of $P_{\mathrm{H}} = 1\,\mathrm{pu}$, indicated as $\delta_{\mathrm{IEL,sat}}$ in the figure.

The consequence of this extended supply is an excessive inertial support, which can unnecessarily increase the energy storage requirements of the converter system. This effect can also have a negative impact on grid frequency restoration dynamics, since P_{H} does not follow the frequency derivative during this time. Finally, the saturation of the angle difference results in the IEL

losing its damping ability during the ROCOF. Thus, the excessive angle difference causes the IEL to lose control over P_H while $|\delta_\mathrm{IEL}| > \delta_\mathrm{IEL,sat}$, which is undesirable.

III. IEL Modifications for Improved Performance

To improve the IEL behaviour in the areas described in the previous section, three modifications of the IEL are suggested in this section. They are shown in Fig. 6a – 6c with the changes to the basic controller from Fig. 3 highlighted in red.

A. Angle-Based IEL

From (7) follows that the sine-function introduces a non-linearity into the IEL, which limits the maximum ROCOF. Replacing $\sin\delta_\mathrm{IEL}$ with an estimation of δ_IEL itself would address this problem. δ_IEL is estimated by using the atan2-function, since it correctly estimates the sign of δ_IEL and is insensitive to changes in the grid voltage magnitude. Using atan2 without further adaptations increases the linear control range up to an angle difference of ±180°, where the estimated angle will switch its sign.

The derivations in [4] resulting in the presented tuning of the IEL assume $v_\mathrm{gq,IEL}$, not δ_IEL as the IEL input. However, $\delta_\mathrm{IEL,sat}$ can be considered small for values of L_f that are typical for grid-connected converter system. Thus, replacing the IEL input as described here will not have a significant impact on the inertial response.

B. Saturation Feedback

The two problems described in the previous section are both caused by δ_IEL exceeding $\delta_\mathrm{IEL,sat}$ (or $P_\mathrm{H}+P_\mathrm{set}$ exceeding P_lim, which is equivalent). Because of this, a feedback of the difference between the unlimited and the limited active power references $P^* - P^*_\mathrm{lim}$ can be used to mitigate these problems. Ideally, the angle difference should saturate as little as possible, which is why the usage of a gain K_fb in the feedback path is advised. An excessive gain on the other hand has a negative impact on dynamic behaviour and stability. The best choice for this gain is system dependent, but for the simulated setup a gain of $K_\mathrm{fb} = 100$ has been proven a good choice and is used here.

C. Auxiliary PI-Controller

The third modification suggestion is based on the idea to use a second, parallel PI-controller with larger gains to speed up the tracking capability of the IEL during saturation. The higher bandwidth of the auxiliary PI-controller allows the angle estimate to stay close

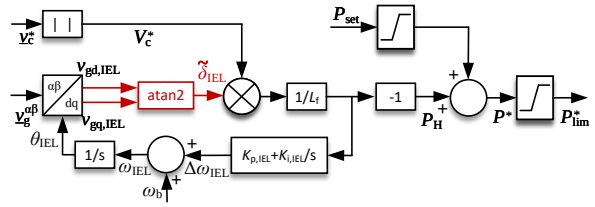

(a) Angle-based IEL adaptation.

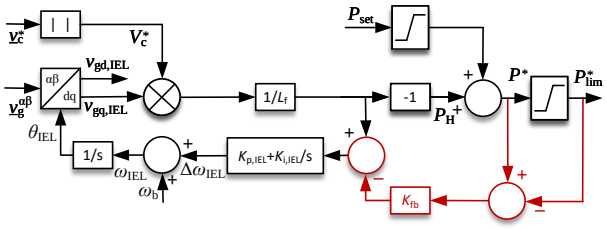

(b) Saturation feedback IEL adaptation.

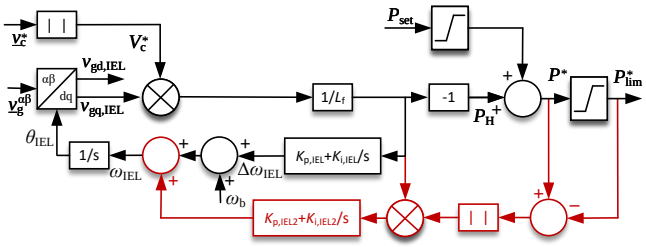

(c) IEL adaptation with auxiliary PI-controller.

Fig. 6: IEL modification suggestions.

to $\delta_\mathrm{IEL,sat}$ to prevent both instability and the negative effects of operation under power limitation. To ensure that the auxiliary PI-controller is only active during saturation, its input is scaled with the absolute value of the difference between unlimited and limited active power reference $|P^* - P^*_\mathrm{lim}|$. Using this difference as a scaling factor instead of adding it to the input signal ensures smooth insertion and removal of the second PI. It should be noted that the integrators of both PI controllers are always active, even when not in limitation. To achieve its goal to keep δ_IEL as close to $\delta_\mathrm{IEL,sat}$ as possible during limitation, the auxiliary PI should have a significantly higher bandwidth than the original IEL. For the cases in this paper, the gains were tuned as for an IEL with an inertia $H = 0.05\,\mathrm{s}$.

The insertion of the second PI is equivalent to adapting the inertia constant of the IEL to exactly the value that, with the given active power headroom and ROCOF, can be provided. However, this adaptation does first occur when limitation is reached, meaning that the initial inertial response is not affected. An advantage of this solution is that the damping provided by the IEL can be adapted through the tuning of the second PI. This

TABLE II: System and control parameters for the simulations.

System parameters		Control parameters	
S_N	1 kVA	L_{v1}	0.35 pu
V_N	100 V	R_{v1}	0.235 pu
ω_N	314.16 rad/s	α_{APL}	2π 15 rad/s
R_f	0.015 pu	α_{CC}	2π 500 rad/s
SCR	10	α_{VC}	2π 1 rad/s

allows to provide additional damping during saturation without slowing down the initial inertial response, which would be the case if the damping ratio of the IEL is increased instead. For this reason, a higher damping ratio was chosen for the auxiliary PI-control ($\xi = 1$).

IV. Simulation Results

The performance of the proposed modifications is investigated using time-domain simulations of the complete system shown in Figs. 1 to 2. For these simulations, the parameters from Tables I and II are used. α_{APL}, α_{CC} and α_{VC} are the closed-loop bandwidth used to tune the APL, current controller and voltage controller, respectively. According to (8), for the simulated inertia constant of $H = 50\,\text{s}$ the critical ROCOF causing instability is ±3.33 Hz/s. To replicate the instability and the consequences of saturated operation from Section II, the same cases are simulated: First, a ROCOF of −3.75 Hz/s that causes instability in the unmodified IEL; and second, a ROCOF of −3 Hz/s where even the unmodified IEL remains stable.

The simulation results for the higher ROCOF are shown in Fig. 7. The blue curves represented the base model, using the unmodified IEL illustrated in Fig. 3. The ROCOF starts at $t = 0.5\,\text{s}$, and from the middle plot the angle difference passes 90° less than 800 ms later. At this point, the IEL loses track of the grid voltage angle and becomes unstable. It can be seen that all three proposed adaptations are able to maintain stable operation even during this higher ROCOF.

Figure 8 shows the simulation results for the lower ROCOF. Here, even the base model maintains stable operation. However, it can be seen that due to the saturation of the inertial power, the full inertial support continues for approximately 500 ms after the ROCOF has ended. This is due to the fact that the angle difference widely exceeds the angle that is needed for the maximum inertial support, $\delta_{IEL,sat} = -8.6°$ (marked in green in the second plot), and that the decrease in the angle difference is not reflected in a decrease of inertial response as long as $|\delta_{IEL}| > \delta_{IEL,sat}|$.

The results for the angle-based IEL described in Section III.A are given in red. They show that the angle

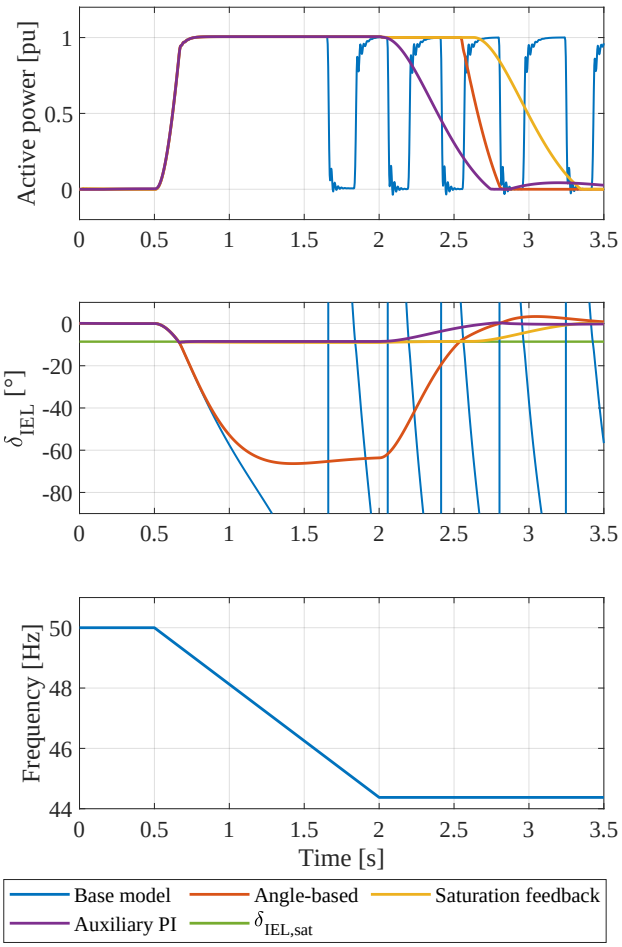

Fig. 7: Simulated active power (top), angle difference (middle) and frequency (bottom) for a ROCOF of −3.75 Hz/s, causing instability in the base model.

difference remains below 70° for the higher ROCOF, and around 50° for the lower. This difference to the base model can be explained by the elimination of the nonlinearity, resulting in a smaller angle difference for the same ROCOF. Nevertheless, the angle difference is in both cases more than five times higher than $\delta_{IEL,sat}$. In consequence, even in this case the inertial support continues unreduced for about 500 ms after the frequency disturbance ends.

In contrast to this, the addition of a saturation feedback to the IEL as introduced in Section III.B allows to keep the angle very close to $\delta_{IEL,sat}$. In the high ROCOF case, the maximum angle difference for this case is −8.97°, only 0.37° larger than $\delta_{IEL,sat}$. Although the inertial power reference barely saturates, the simulation results show that the injection of excessive power due to operation under saturation is even worse than in the two cases discussed previously. This can be explained by the fact that the feedback increases the impact of the

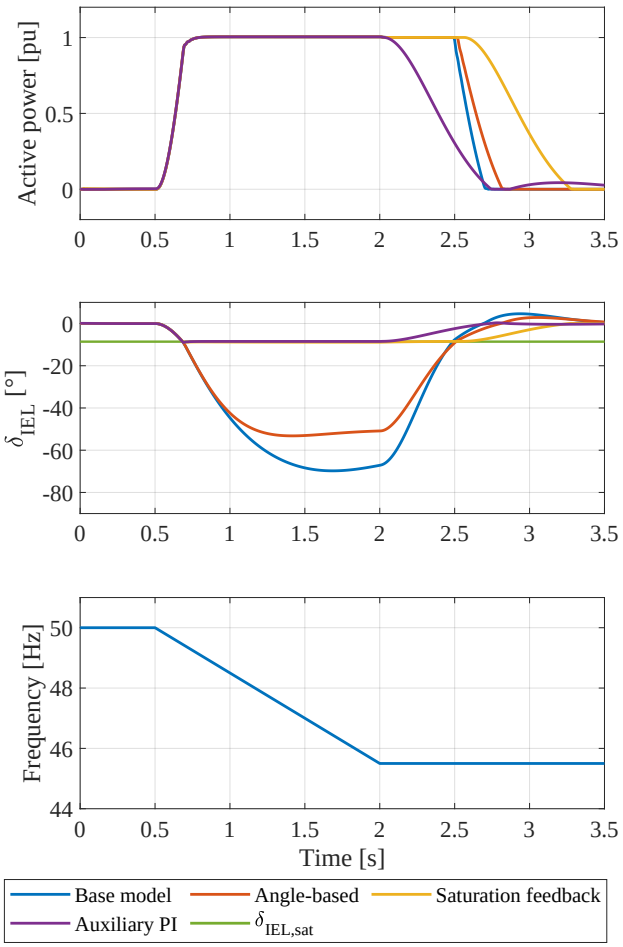

Fig. 8: Simulated active power (top), angle difference (middle) and frequency (bottom) for a ROCOF of −3 Hz/s, a stable case in the base model.

proportional part of the IEL's PI controller, and reduces the integral part's. This means that, with this adaptation, the integrator state differs more from the actual grid frequency as in the previously discussed solutions. As the ROCOF ends, the additional input into the PI from the saturation feedback subsides, which results in additional time required for the IEL to eliminate the angle difference. A study of different gains has shown that the post-disturbance performance of this approach cannot be improved significantly by varying K_{fb}.

The final modification suggestion is the introduction of an auxiliary PI-controller as described in Section III.C. The results of this case are shown as purple curves. The angle difference remains even closer to $\delta_{\mathrm{IEL,sat}}$ than for the saturation feedback, but in this case, the inertial response starts to reduce as soon as the ROCOF is removed. This means that the IEL maintains control throughout the whole disturbance, because the state of the auxiliary integrator is kept active, even as P_{H} drops

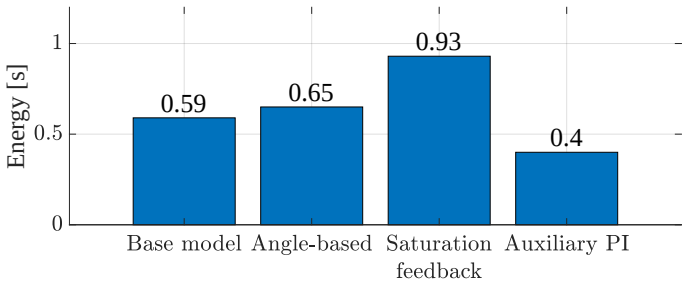

Fig. 9: Energy injected after disturbance end.

below its limit. In consequence, not only the angle difference is kept close to its saturation limit, but the IEL's estimate of the grid frequency is kept accurate throughout the disturbance.

The energy injected to the grid during the frequency disturbance is the same for all simulated cases, but the amount injected after the end of the disturbance varies significantly. Since the ROCOF has ended at this point, additional inertial support can be considered superfluous, and the goal is to reduce the unnecessary inertial support. Figure 9 shows the energy that is injected after the disturbance has ended for all four controller variants, where an energy of 1 s corresponds to the injection of 1 pu power for the duration of 1 s. The data confirm that the auxiliary PI results in the least additional energy injected, achieving a reduction of 33 % from the base model.

The active power plots in Figs. 7 and 8 show that the inertial power at the beginning of the disturbance increases much faster than it decreases in the end. This is the case even for the best modification, the auxiliary PI-controller. This effect is caused due to the de-facto limitation introduced by the second PI: At the beginning of the disturbance, the ROCOF causes the grid voltage and the internal IEL angle to separate. Without addition of the second PI controller, this would result in the same angle difference as shown for the base model. Consequently, the angle follows the shape of a step response ending in a final value of approximately 70°. But as soon as $\delta_{\mathrm{IEL,sat}}$ is reached, the second PI with a much higher bandwidth is introduced, which in effect limits the angle difference to this value. This means that the step response is terminated here, and only the first part of the rise is visible. The end of the disturbance, on the other hand, is an uncut step response from δ_{IEL} down to zero. As this step is much smaller than the (unlimited) one at the beginning of the disturbance would be, the same rise time results in a flatter response.

The impact of the second PI is in this aspect of the response limited to maintaining the angle difference

close to $\delta_{\mathrm{IEL,sat}}$. This becomes obvious when comparing to the base case. At the end of the disturbance the angle difference in the base case reduces with the same steepness as at the beginning. Nevertheless, this reduction is not visible in the inertial response before the angle difference reaches $\delta_{\mathrm{IEL,sat}}$ again due to the saturation. Because the rise time of the control loop is the same in both cases, the inertial response from both the base case and the auxiliary PI-control reaches zero again at approximately the same time, circa 650 ms after the disturbance ends. Even so, the IEL with an auxiliary PI starts reduction immediately, which reduces the amount of unnecessary energy injection and reflects an improved control performance.

V. Conclusions

This paper has shown that the original IEL design from [4] is very robust and is prone to instability only under extreme operating conditions far beyond the limits of today's power grids. The analysis has also revealed that for large ROCOFs, the saturation of the inertial support and IEL angle difference causes the inertial power to not follow the ROCOF while in saturation, even when stability is maintained. This operation under power limitation results in an undesirable power injection after the disturbance ends.

This motivated the proposal, investigation and comparison of three solutions to improve the robustness and controllability of the IEL. The simulation results show that of these suggestions, only the addition of an auxiliary PI-controller is able to mitigate both problems. This adaptation is equivalent to immediate dynamic scaling of the IEL's inertia constant based on ROCOF and headroom when the active power limit is hit, and is able to improve the IEL robustness notably without having an impact on the initial inertial response. The auxiliary PI also makes it possible to dynamically change the IEL damping during limitation. Based on these observations, it is advisable to include the auxiliary PI-controller in the IEL.

References

[1] J. Matevosyan *et al.*, "Grid-Forming Inverters: Are They the Key for High Renewable Penetration?" *IEEE Power and Energy Magazine*, vol. 17, no. 6, Nov. 2019.

[2] ENTSO-E, "High Penetration of Power Electronic Interfaced Power Sources and the Potential Contribution of Grid Forming Converters," 2020.

[3] B. Fan *et al.*, "A Review of Current-Limiting Control of Grid-Forming Inverters Under Symmetrical Disturbances," *IEEE Open Journal of Power Electronics*, 2022.

[4] P. Imgart *et al.*, "A Cascaded Power Controller for Robust Frequency Ride-Through of Grid-Forming Converters," presented at the 2022 IEEE Energy Conversion Congress and Exposition (ECCE), Detroit, MI, USA, 2022.

[5] A. Narula *et al.*, "Voltage-based Current Limitation Strategy to Preserve Grid-forming Properties Under Severe Grid Disturbances," *IEEE Open Journal of Power Electronics*, 2023.

[6] M. D. Librandi *et al.*, "Local Frequency Transients in the Future European Synchronous Transmission Grid," in *NEIS 2021; Conference on Sustainable Energy Supply and Energy Storage Systems*, Sep. 2021.

[7] S. K. Chaudhary *et al.*, "Islanded Operation of Offshore Wind Power Plant using IBESS," in *2021 IEEE Power & Energy Society General Meeting (PESGM)*, Jul. 2021.

[8] P. Kundur, *Power System Stability and Control* (The EPRI Power System Engineering Series), N. J. Balu and M. G. Lauby, Eds. New York: McGraw-Hill, 1994.

[9] P. Imgart *et al.*, "An Overview of Grid-Connection Requirements for Converters and Their Impact on Grid-Forming Control," *EPE'22 ECCE Europe*, 2022.

[10] ENTSO-E *et al.*, "Future system inertia 2," 2018.